CHAPTER IV

RESULTS AND DISCUSSIONS

CHAPTER IV

RESULTS AND DISCUSSIONS

In this section, the simulation results of the proposed approach are discussed.

4.1 SIMULATION RESULTS AND DISCUSSION ON CONTRAST ENHANCEMENT USING MODIFIED SIGMOID FUNCTION

The proposed algorithm was applied to various color real sports images. Figure 35 shows the original sports image. A tennis image was taken as the test image. Figure 36 shows the averaging filtered output and Figure 37 shows the preprocessed output using unsharp masking. From the outputs it was clear that the edges of the original image were enhanced in this preprocessing step.

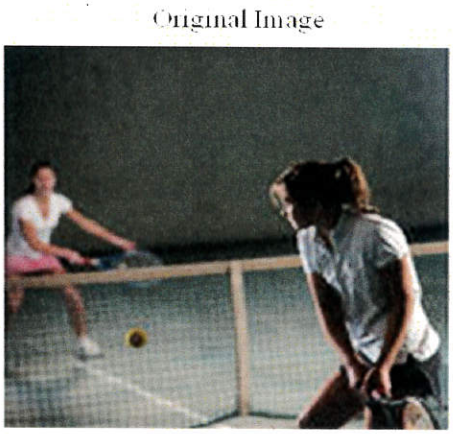

Figure – 35: Original Tennis Image with poor lighting.

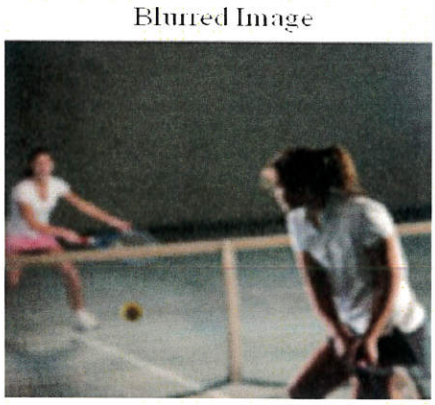

Figure – 36: Blurred Image obtained using Averaging Filter

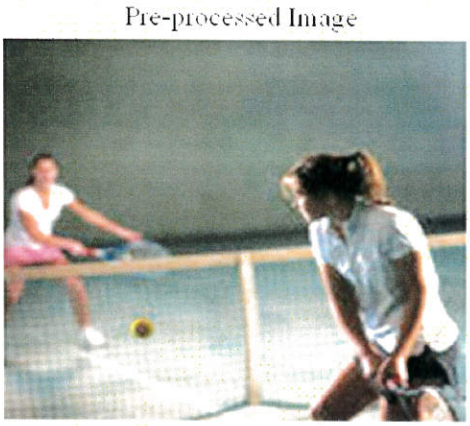

Figure – 37: Preprocessed Image using Unsharp Masking

The pre-processed image was enhanced using modified sigmoid mapping function. Figure 38 shows the output with c=5 and threshold =0.3. The threshold value was fixed based on the input image. Figure 39 shows the output with c=8 and threshold =0.3. Figure 40 shows the output with c=10 and threshold =0.3. In this analysis the threshold value was maintained constant and the contrast factor was increased. Thus from the results it was clear that when the contrast factor value was increased, the overall contrast of the image becomes better and more details were visible.

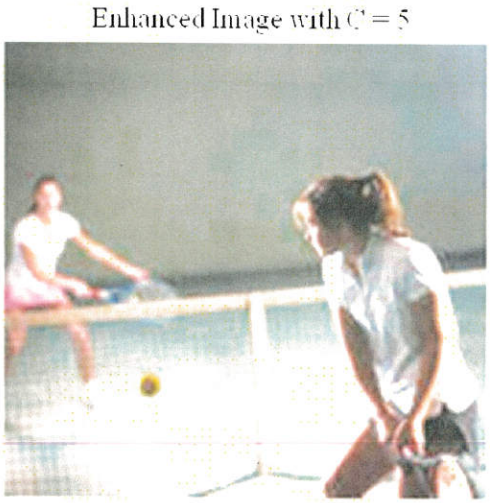

Figure – 38: Enhanced Image using c=5 and th=0.3

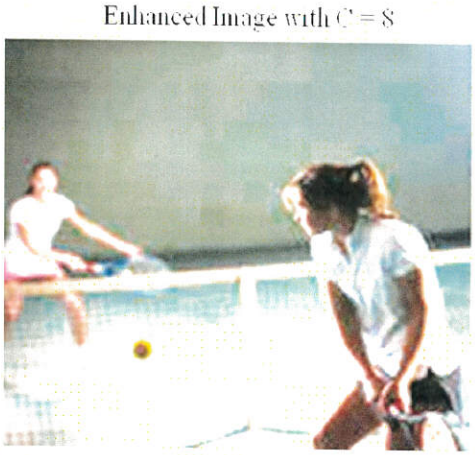

Figure – 39: Enhanced Image using c=8 and th=0.3

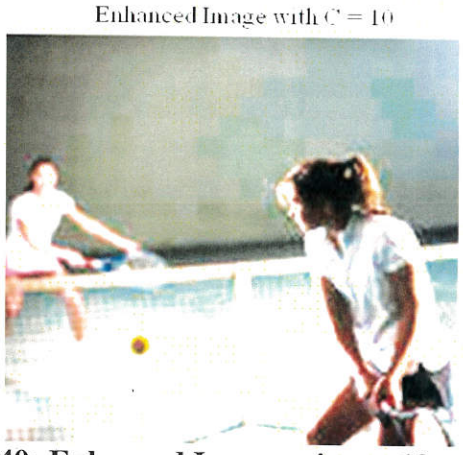

Figure – 40: Enhanced Image using c=10 and th=0.3

The proposed algorithm was applied to two other images and the results were shown. Figure 41(a) shows the original football match image and 41(b) the preprocessed image after unsharp masking. Figure 41(c) shows the contrast enhanced image using modified sigmoid mapping function with contrast factor c=5. Figure 41(d) was same as 41(c) but contrast factor c increased to 8. Figure 42 shows the same processes performed on the third test image. The original image was a tennis match image, shown in Figure 42(a), Figure 42(b) shows the preprocessed image after unsharp masking. Figures 3.7 (c) & (d) show the contrast enhanced images using modified sigmoid mapping function with contrast factor c=5 & 8 respectively. As

compared to the original image the enhanced images give more visual details and also the contrast was enhanced.

(a) Original Football Image

(b) Preprocessed Image

(c) Contrast Enhanced image with C=5

(d) Contrast Enhanced image with C=8

Figure – 41: Contrast Enhancement of football image

(a) Original Tennis Match Image

(b) Preprocessed Image

(c) Contrast Enhanced image with C=5

(d) Contrast Enhanced image with C=8

Figure – 42: Contrast Enhancement of tennis image

TABLE – XVI

PERFORMANCE ANALYSIS OF THE PROPOSED METHOD

Test Image	Tennis Image with Mean Min= 0.2654		Football Image with Min=0.3705		Tennis Court Image with Mean Min= 0.3192	
Enhancement Method Used	**Average Intensity**	**Measure of Contrast**	**Average Intensity**	**Measure of Contrast**	**Average Intensity**	**Measure of Contrast**
Contrast Stretching	0.444051	0.6731	0.3850	0.0390	0.53	0.6684
High boost Filtering	0.55708	1.0990	0.4864	0.3128	0.6745	1.1130
Gamma Correction	0.3361	0.2664	0.4620	0.2468	0.5523	0.7300
Sigmoid Function	0.4272	0.6096	0.4102	0.1072	0.4112	0.2882
Modified Sigmoid Function C=5	0.6214	**1.3414**	0.5627	**0.5188**	0.7291	**1.2841**
Modified Sigmoid Function C=8	0.6471	**1.4382**	0.5758	**0.5541**	0.8038	**1.5181**
Modified Sigmoid Function C=10	0.6565	**1.4736**	0.5797	**0.5646**	0.8370	**1.6221**

4.2 SIMULATION RESULTS AND DISCUSSION ON CONTRAST ENHANCEMENT USING FUZZY RULES

Figure 43 shows the results obtained using modified sigmoid function. Figure 43(a) shows the original image Img-3. For this image the threshold value was chosen as 0.3 and the contrast factor value was varied and the results were obtained. Figures 43(b), 43(c) and 43(d) show the enhanced image obtained for a contrast factor of 5, 8 and 10 respectively. From the results it was clear that as the contrast factor increases the image enhancement also increases but for contrast factor value greater than 10 the image tends to show a glared effect. For a contrast value of 5 the resulting image has

got a dull washed out look, thus the optimal value for the contrast factor would be between 6 and 10.

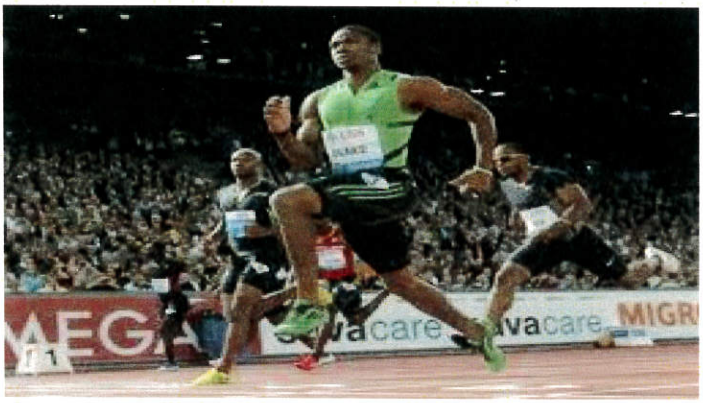

a) Original Image – Img-3

b) Enhanced Image using Modified Sigmoid Function of C=8, Th=0.3

c) Enhanced Image using Modified Sigmoid Function of C=8 ,Th=0.3

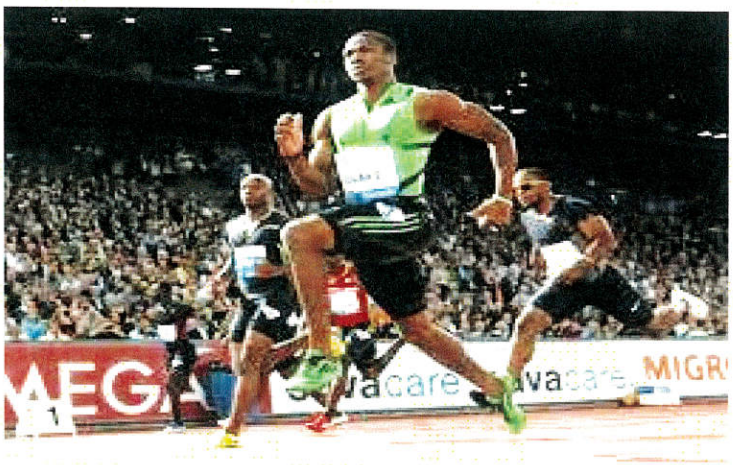

d) Enhanced Image using Modified Sigmoid Function of C=10, Th=0.3

Figure – 43: Contrast Enhancement using Modified Sigmoid Function

Contrast by definition, was a psychophysical non-measurable characteristic. On the other hand, de-facto, it was a quantitative parameter essential for digital image processing and algorithm developers have to use some formula for Contrast measure. There was no conventional measure for contrast, however to evaluate the contrast enhancement performance of our method, the following evaluation parameter have to be considered.

Several sports images were taken for the purpose of experimentation and the contrast enhanced results were obtained using the methods described above. Histogram Equalization method though has shown better measure of contrast than fuzzy rule based method for some of the images, it was seldom used because of the disadvantages discussed earlier. The measure of contrast obtained for a sample of 8 test images is shown in Table XVII and is also plotted in the graph shown in Figure 44. From the table and the graph it was clear that the measure of contrast was high for the modified sigmoid function compared to the fuzzy rule base method and Histogram Equalisation. A very high Measure of Contrast was obtained for the

modified sigmoid function with contrast factor C=10. When the contrast factor value was increased beyond that the image gets a glare effect. Thus the optimal value for the contrast factor would be between 6 and 10. Thus the two proposed methods for contrast enhancement using modified sigmoid function shows good results and can be used as an effective method for contrast enhancement of color images.

$$\text{Measure of Contrast} = \frac{M_{en} - M_{in}}{M_{in}} \qquad (4.1)$$

Where

M_{en} - was the average intensity value of the enhanced image

M_{in} - was the average intensity value of the original input image

TABLE – XVII

MEASURE OF CONTRAST

Enhancement Method	Img1	Img2	Img3	Img4	Img5	Img6	Img7	Img8
Histogram Equalization	0.672	0.345	0.684	0.852	0.742	0.832	0.432	0.544
Fuzzy Logic	0.785	0.586	0.7402	0.6904	0.862	0.796	0.396	0.592
Modified Sigmoid Function , C=5	1.012	0.889	1.182	0.764	1.002	1.2106	0.684	0.7846
Modified Sigmoid Function , C=8	1.208	0.974	1.358	0.884	1.24	1.528	0.7132	0.8192
Modified Sigmoid Function , C=10	1.346	1.056	1.624	0.962	1.396	1.6691	0.8254	0.943

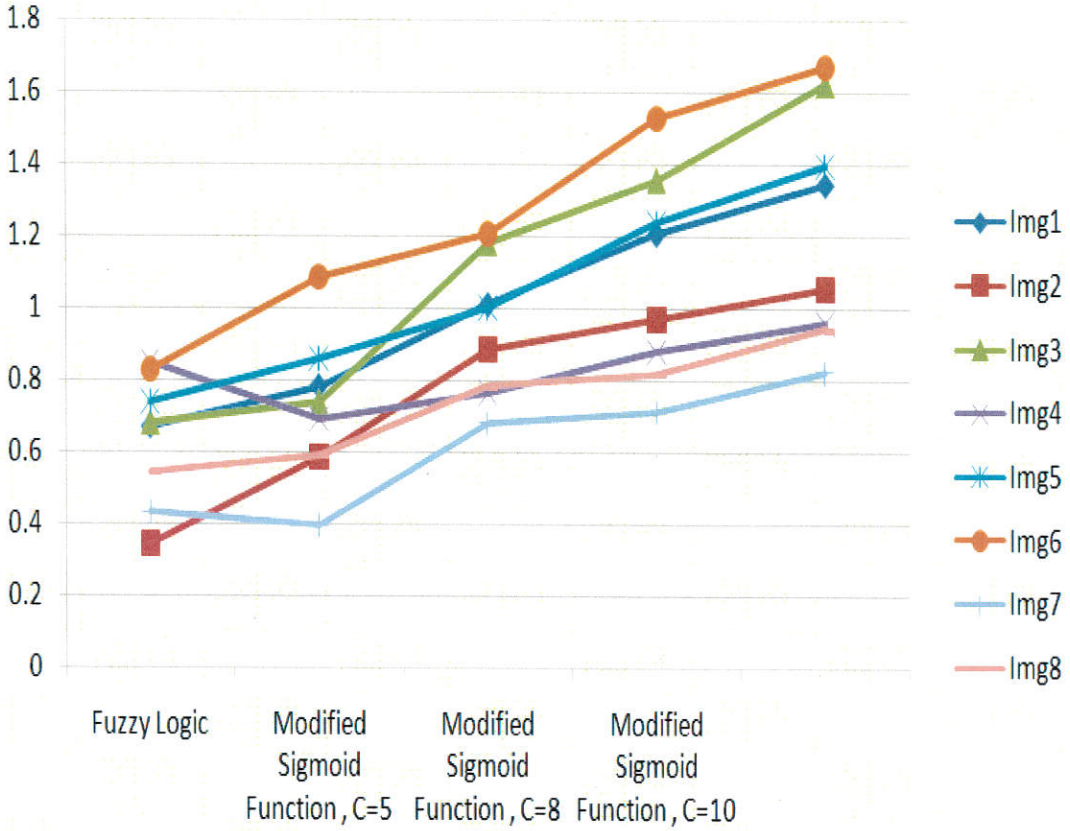

Figure – 44: A plot of Measure of Contrast for various images

Contrast enhancement of color sport images has gained importance recently with the advent in sports image processing. In this thesis two different approaches for contrast enhancement of dark sports images were discussed. Performance of both the methods was comparatively good against the conventional methods like histogram equalization and contrast stretching. Contrast Enhancement using fuzzy rule based method and modified sigmoid function had shown significant improvement in contrast and proved to be useful for further processing of sports images. Contrast enhancement using modified sigmoid function had the added advantage that it was also flexible, that the contrast factor could be adjusted until satisfactory results were obtained. Discussions and investigations are going on to device a method which can by itself determine the contrast factor and threshold value. Contrast Enhancement of

the color sports image was the first step in the process of analyzing the sports images to determine the performance of the players. Edge detection techniques were being explored for the next stage of analyzing the images.

4.3 RESULTS OF BACKGROUND SUBSTRACTION

The twelve human poses had been considered for the implementation such as A. Standing, B.Right hand rise, C. Left hand rise, D. Both hands rise, E. Right hand up, F. Left hand up, G. Both hands up, H. Right leg rise, I. Left leg rise, J. Right salute, K. Left salute, and L. Crouching as in Figure 45. In this, methods 1,2,3 and 7 were developed based on Gray scale approach whereas methods 4,5,6 and 8 were implemented using RGB computation. The simulation results of gray scale and RGB were shown in Figure 46. From the analysis, method 5(FD+ATU) and method 6(FD+WT) provided better background subtraction.

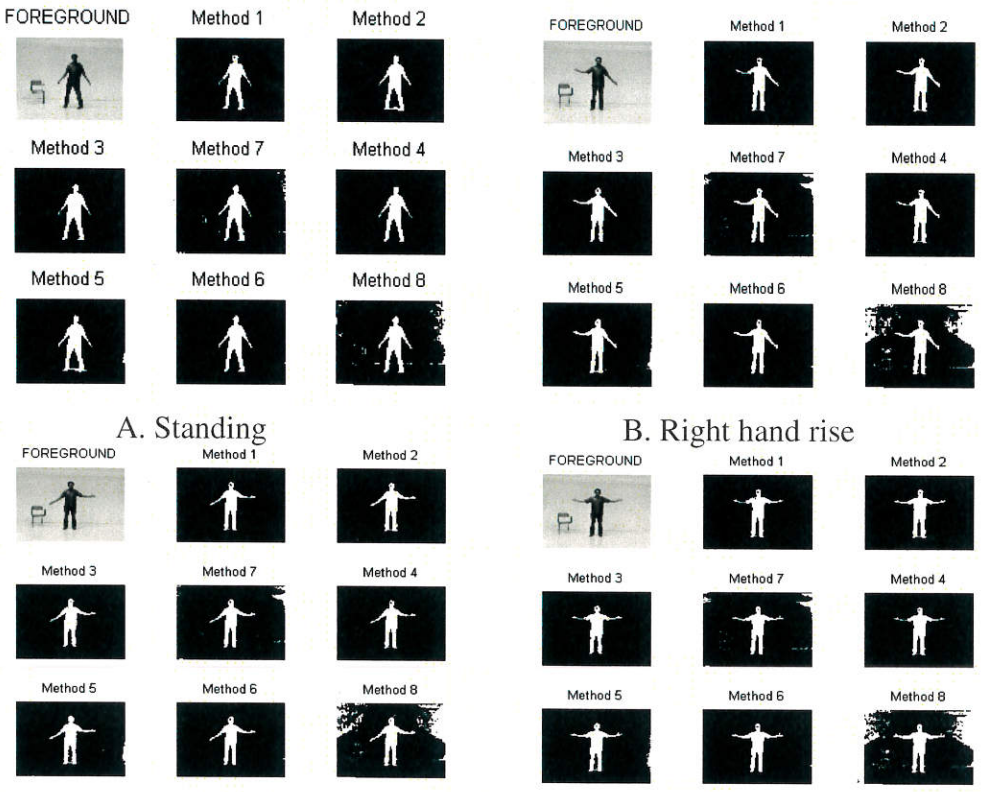

A. Standing

B. Right hand rise

C. Left hand rise

D. Both hands rise

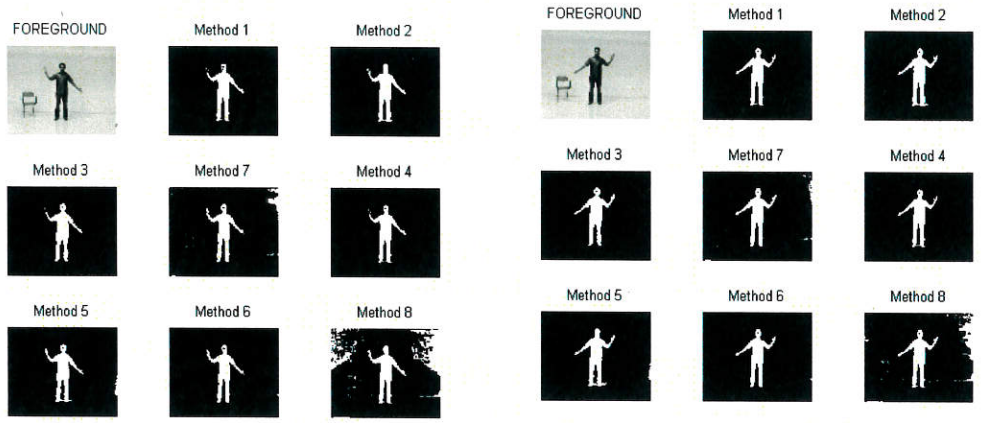

E. Right hand up

F. Left hand up

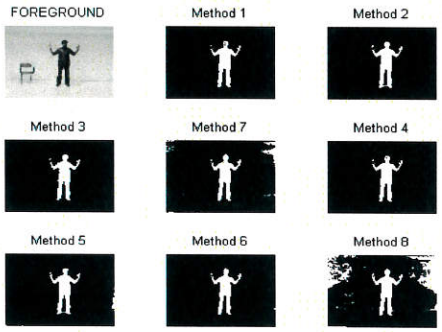

G. Both hands rise

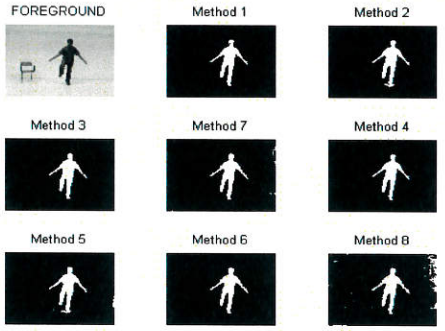

H. Right leg rise

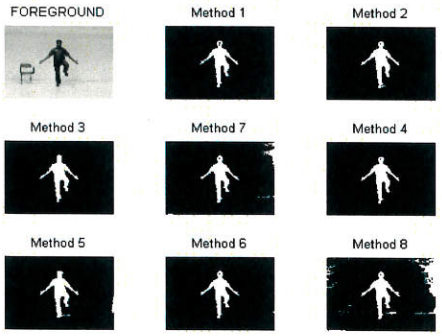

I. Left leg rise

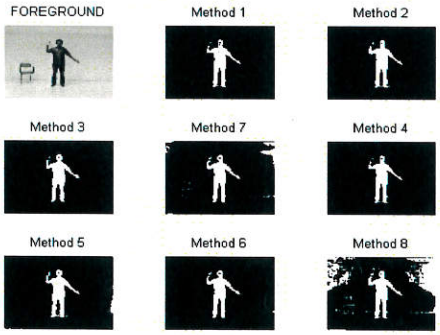

J. Right salute

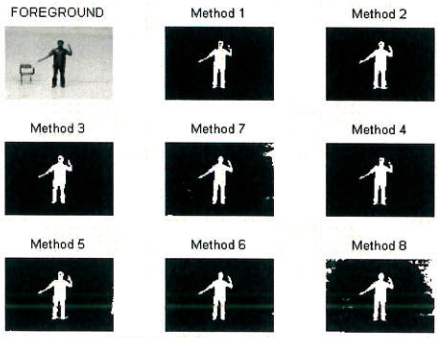

K. Left salute

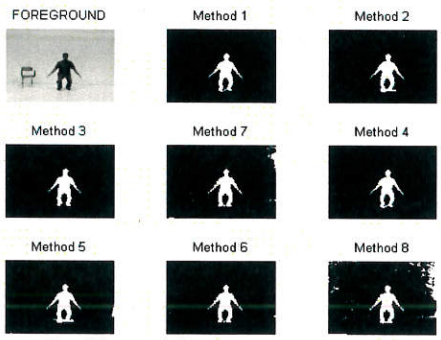

L. Crouching

Figure - 45: Simulation results of background subtraction for different human poses

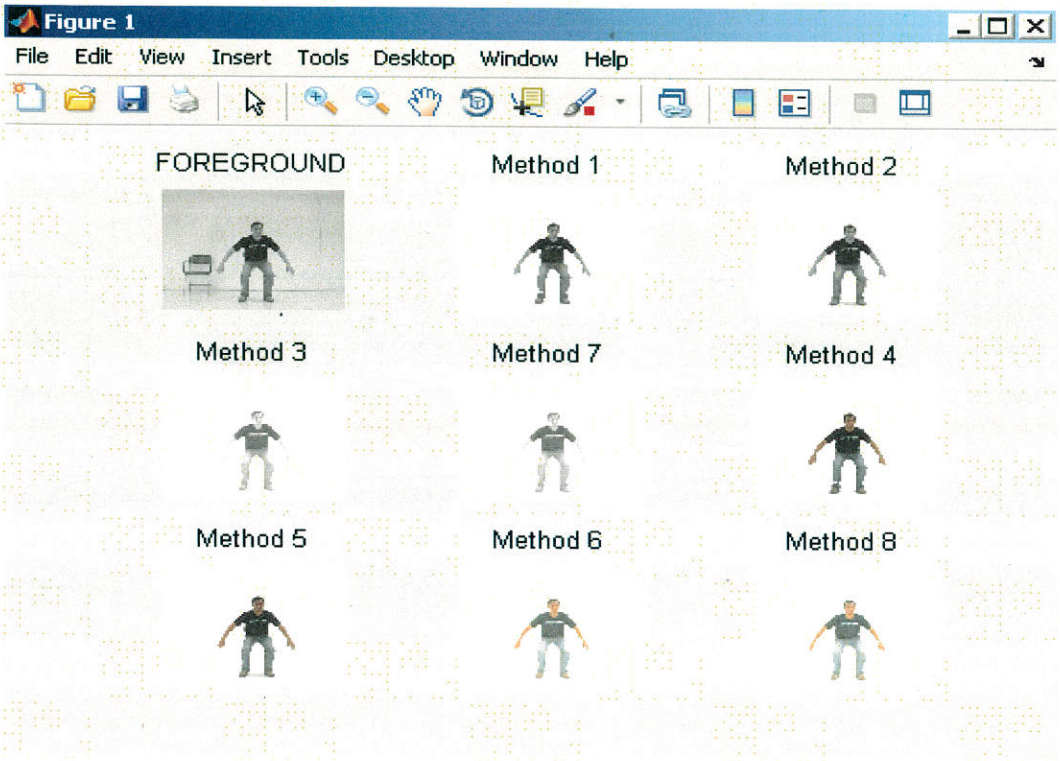

Figure – 46: Simulation results of background subtraction for Gray scale and RGB computation

4.3.1 DISCUSSION ON AUTOMATIC THRESHOLD UPDATION

The threshold values were updated using the proposed approach to get smooth foreground image. This approach was experimented with different threshold values for 50 frames in a sequence. The three threshold levels such as 55, 75 and 100 were considered for the execution. It was seen that the threshold values are adjusted according to the current frames of video. For the bright videos, the levels of threshold values are higher compared to uniform light video which were shown in Figure 47 and Figure 48.

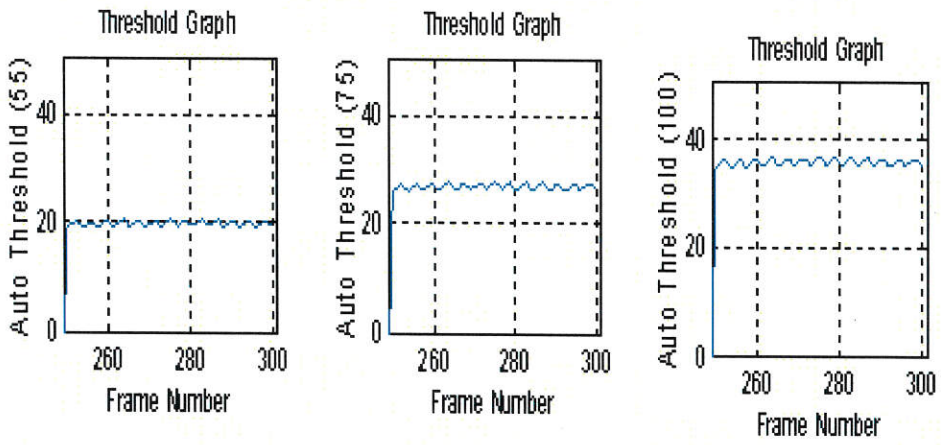

(a)

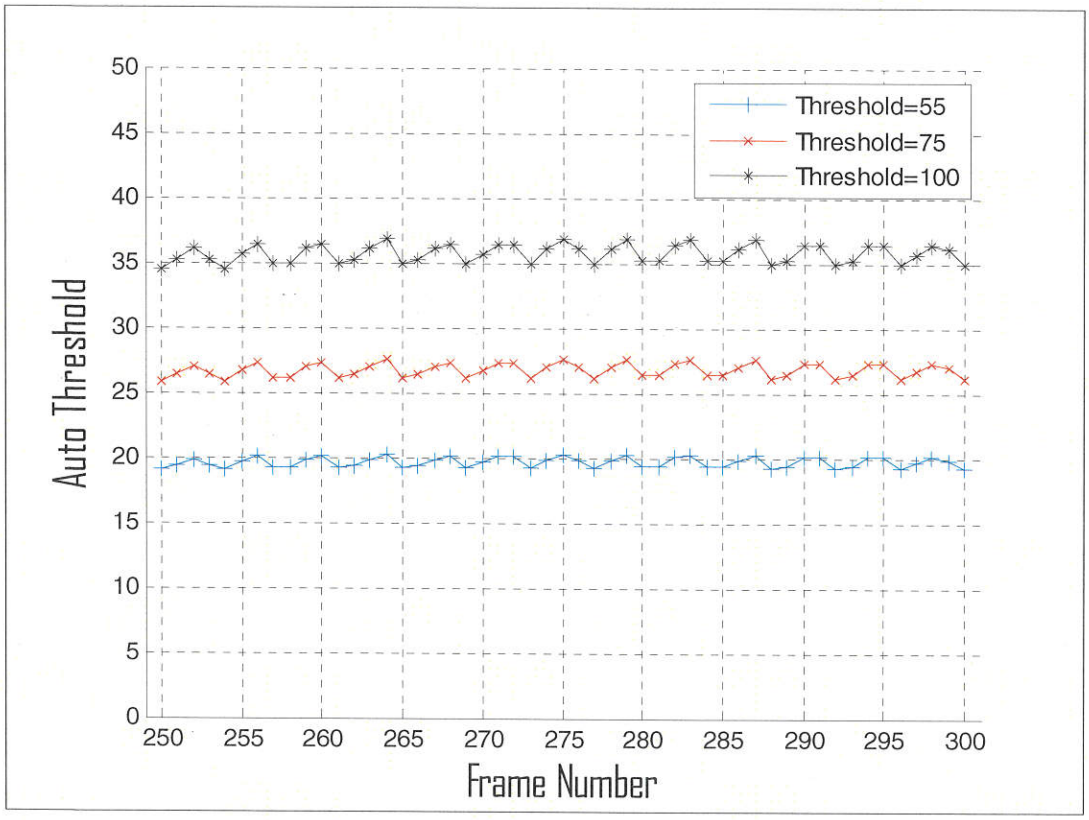

(b)

Figure – 47: Threshold updation for uniform light video
(a) Individual threshold variation (b) Consolidated threshold variation

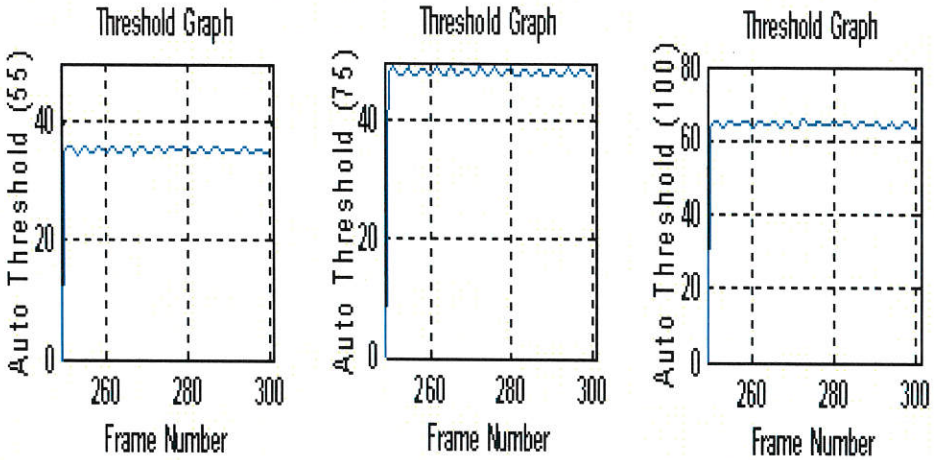

(a)

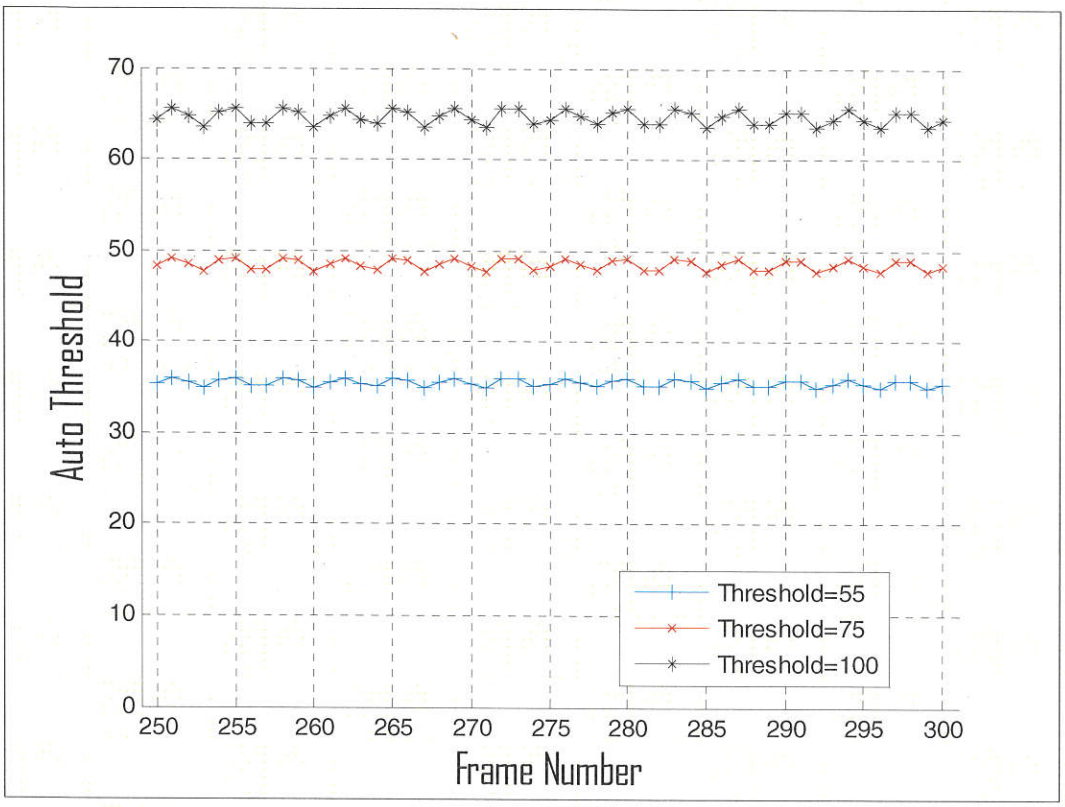

(b)

Figure – 48: Threshold updation for bright light video
(a) Individual threshold variation (b) Consolidated threshold variation

4.3.2 DISCUSSION ON ACCURACY

From the measures of True Positive (TP), True Negative (TN), False Positive (FP) and False Negative (FN), the accuracy was calculated. True positives (TP) was the number of items correctly labeled as belonging to the positive class whereas false positives (FP) was the items that are incorrectly labeled as belonging to the class. True negatives (TN) refers to the correctly rejected among the class whereas False negatives (FN) were the items which were not labeled as belonging to the positive class but should have been. Accuracy was defined as the ratio of sum of true positive and true negative to the sum of true positive, true negative, false positive and false negative by the equation (4.2). It was measured for methods 2 to 8 on a single video as in Figure 49. And average accuracy of 50 frames was also calculated. Here, method 1 was considered as a base for evaluating the measures of accuracy as it holds simplicity and it is widely used. From the analysis of accuracy, method 5 (FD+ATU) and method 6(FD+DWT) produced better performance for background subtraction because of using ATU and DWT with the aid of RGB computation. Figure 50 shows the overall accuracy of videos.

$$\text{Accuracy} = \frac{TP + TN}{TP + TN + FP + FN} \tag{4.2}$$

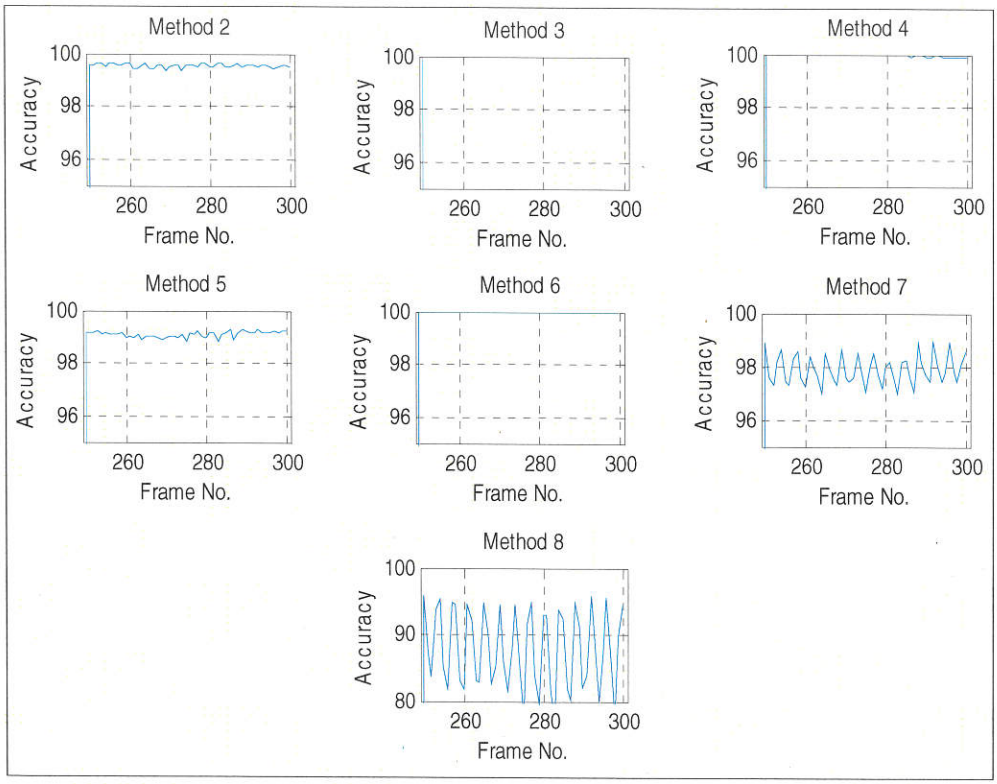

(a)

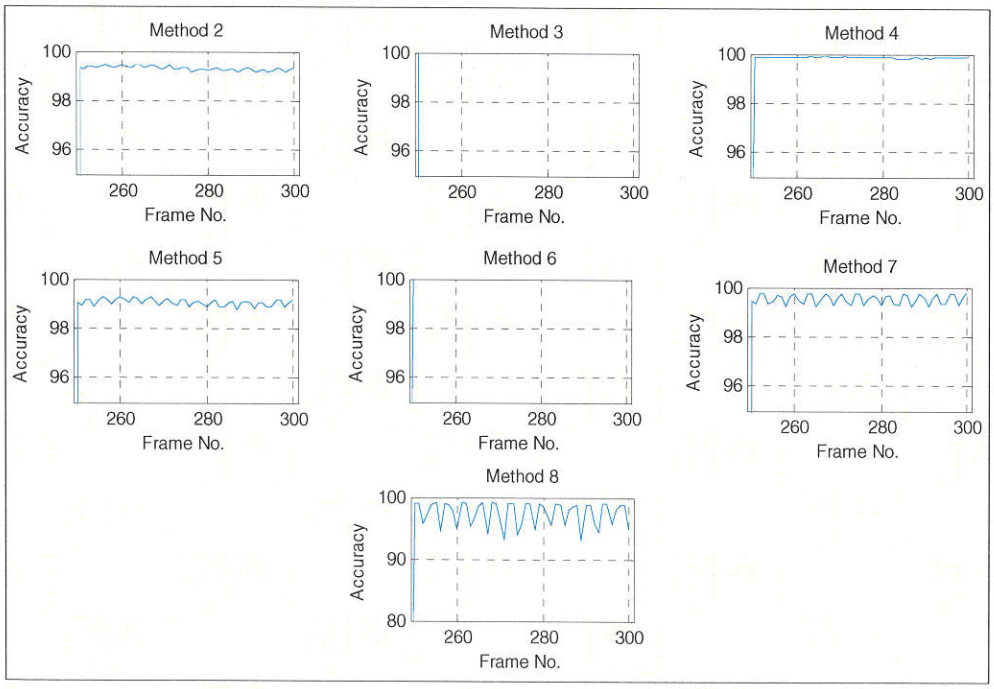

Figure – 49: Computation of Accuracy
(a) For uniform light video (b) For bright light video

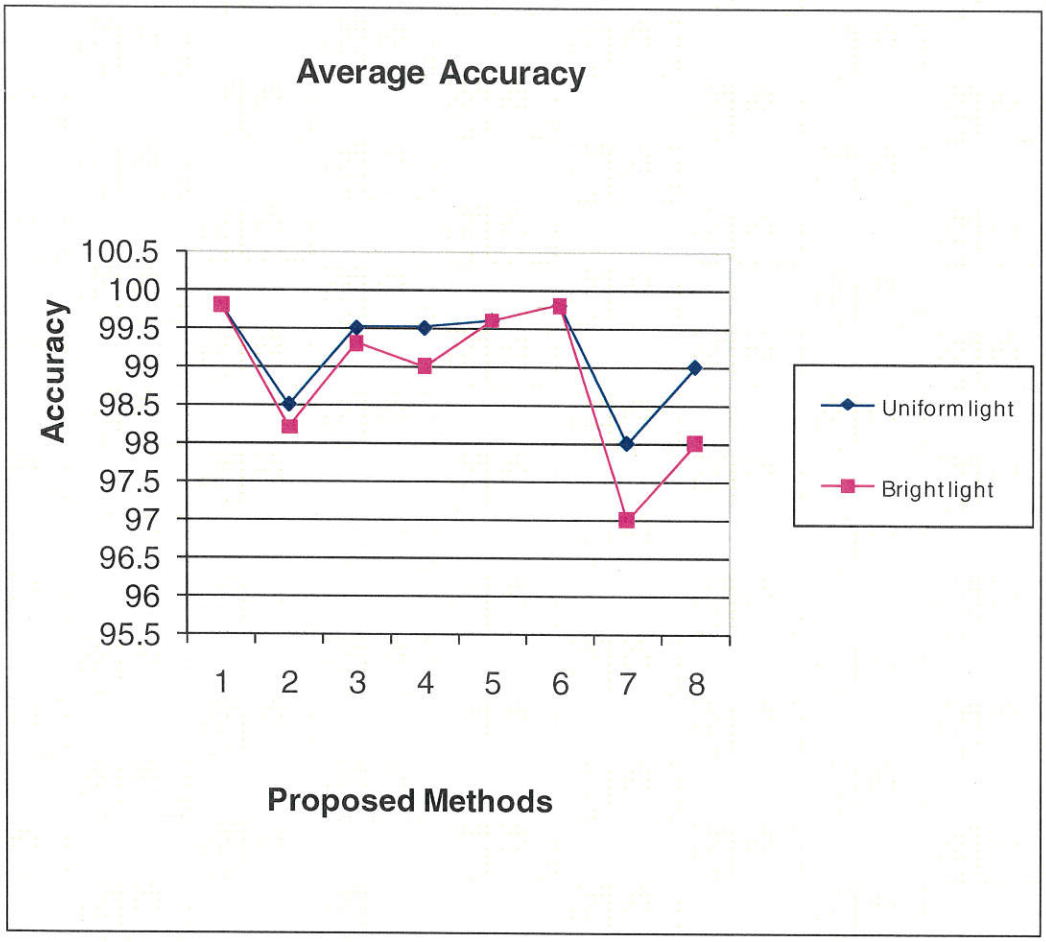

Figure – 50: Average accuracy of background subtraction methods for videos

4.3.3 DISCUSSION ON RUN TIME

In this section, the time required to compute the proposed methods was determined. The 50 frames were taken for the computation from the videos. It was seen that the time computation for uniform light and bright light were same. Here, the run time for method 6 (FD+WT) and method 8(FD+DWT+WT) was lesser than method 4(FD). From this, it was clear that the computation time was reduced when wavelet transform was applied which is shown in Figure 51.

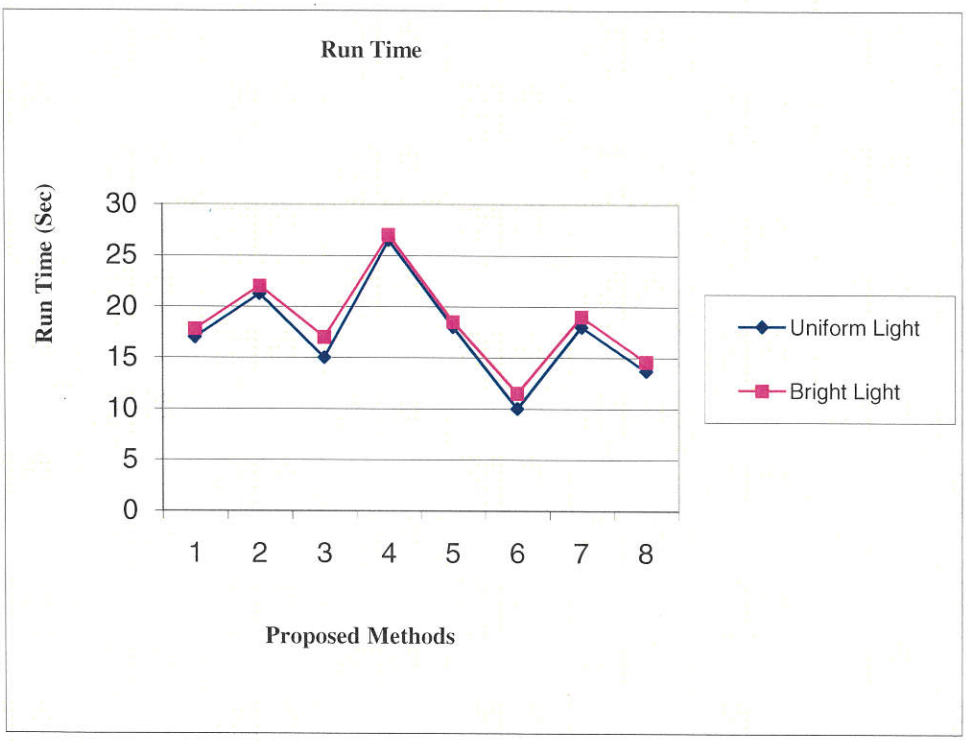

Figure – 51: Run time of proposed methods

4.4 RESULTS OF HUMAN BODY PARTS IDENTIFICATION

Figure 52 shows the results of Video #1 and Video #2 for a single person and multiple persons wearing half sleeve and full sleeve shirts.

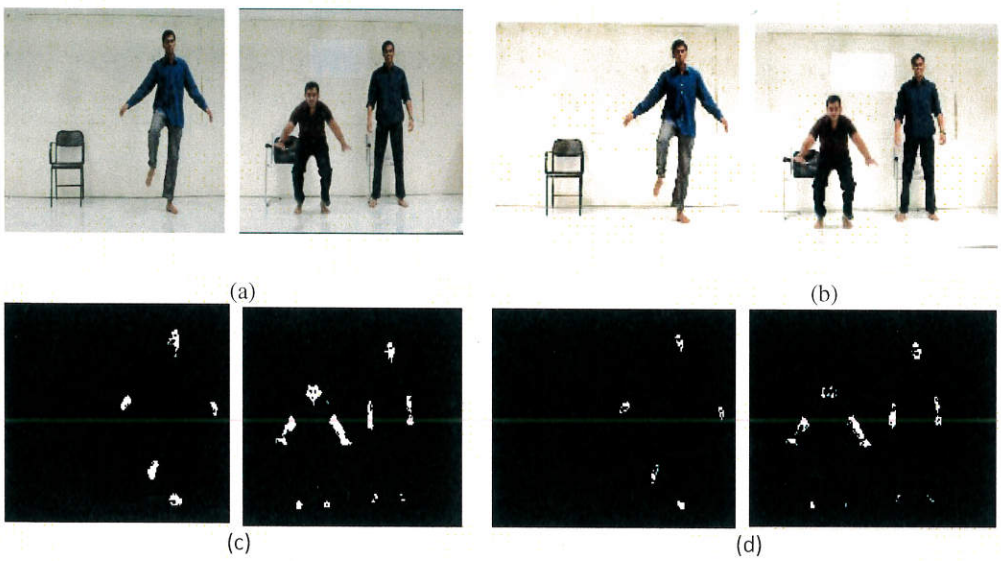

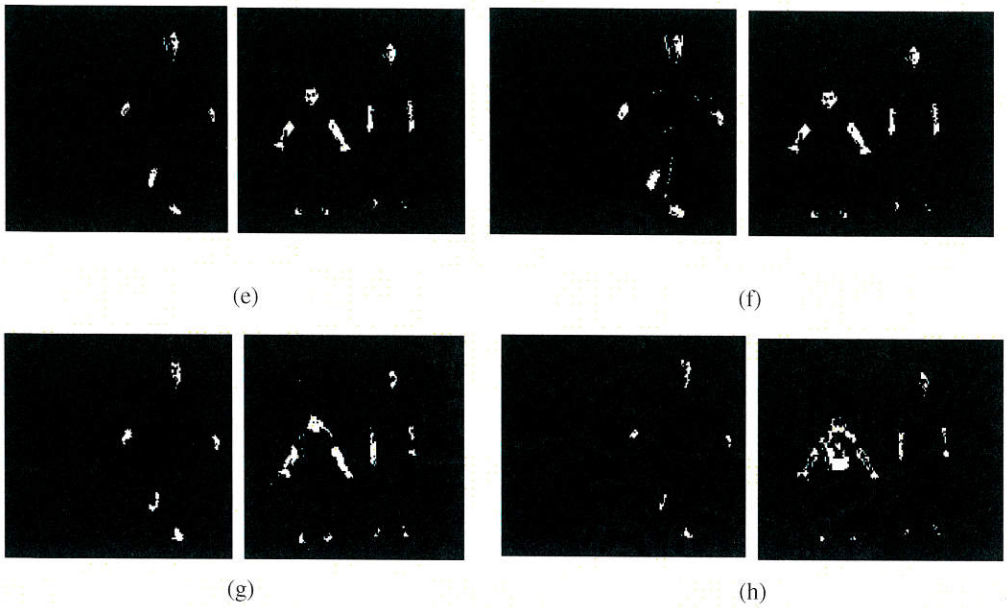

Figure – 52: Results of different color space models(a) Original Video images of Video 1(frame# 512) and Video 2 (frame#495); (b) After Pre-processing; (c) RGB; (d) YCbCr; (e)HSV 1; (f)HSV 2; (g) HSI and (h) Normalized RGB

In the proposed work, the human body parts are tracked for every frame of video sequences. Using the color models, the body parts were identified. Here, the body parts of thirteen human poses were identified which are shown in Figure 53. For this implementation, the proposed algorithm was experimented for different persons and videos with varying clothing conditions.

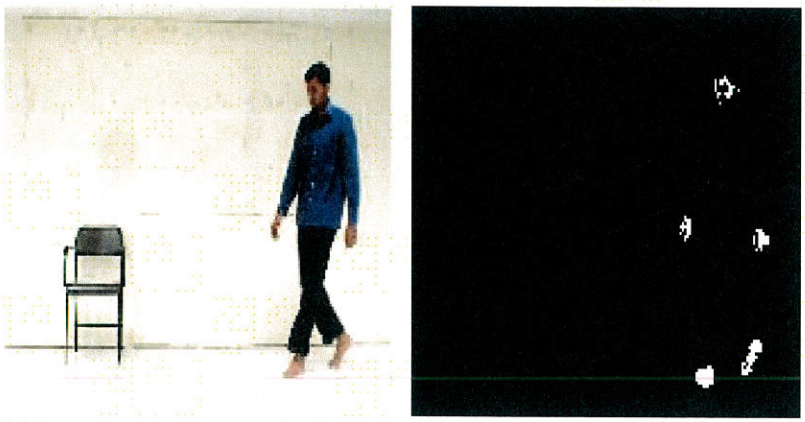

(a)

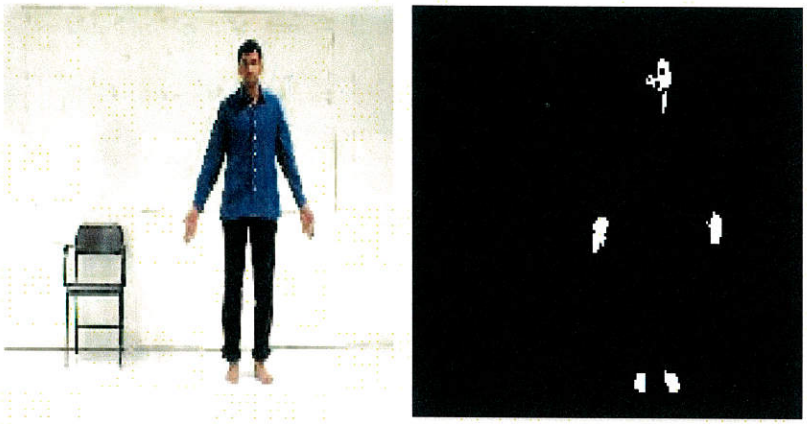

(b)

(c)

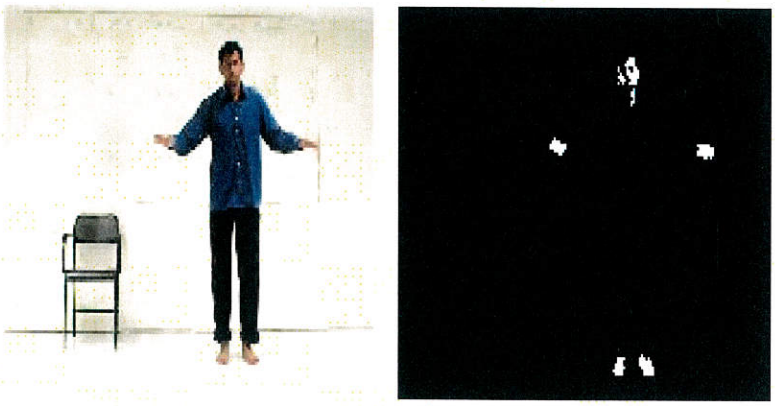

(d)

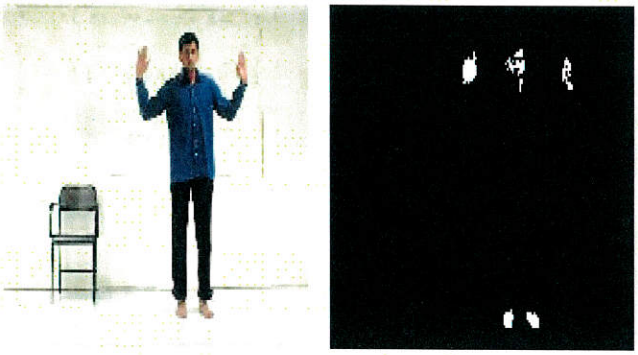

(e)

(f)

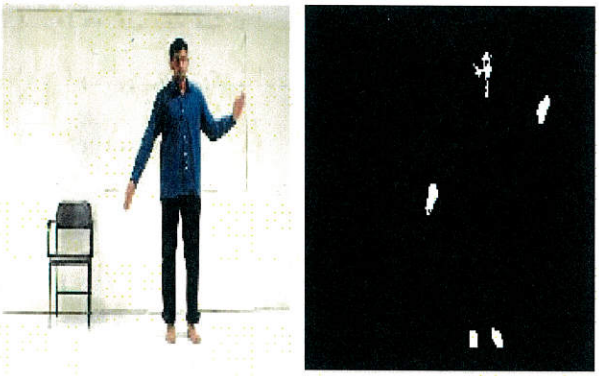

(g)

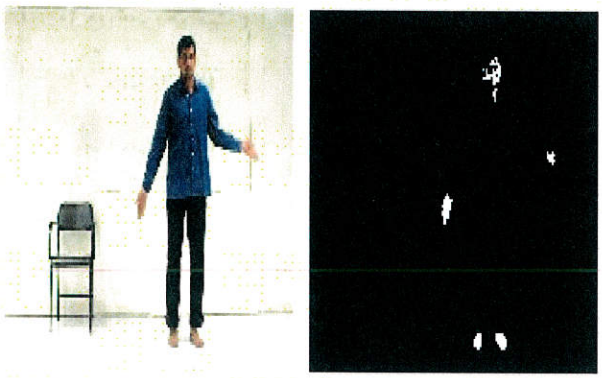

(h)

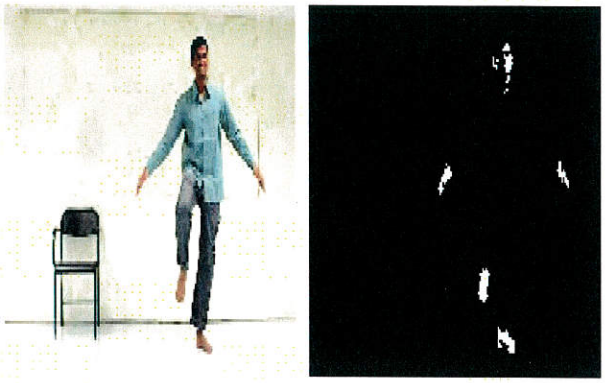

(i)

(j)

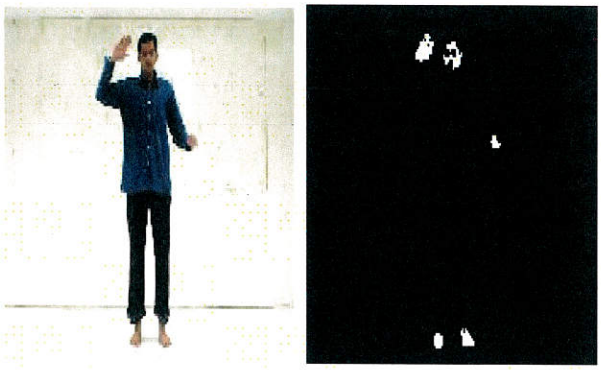

(k)

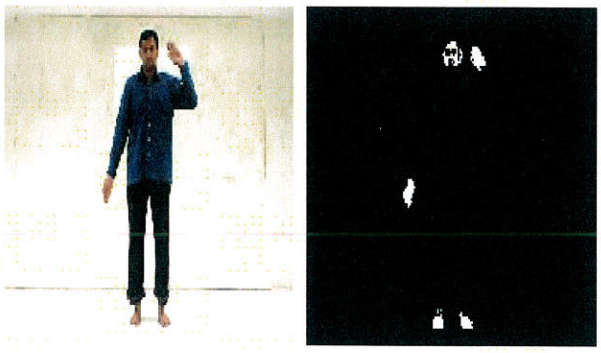

(l)

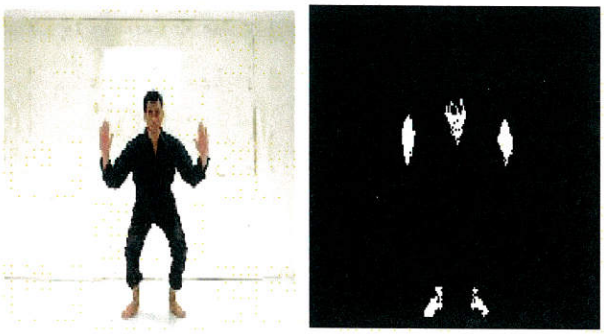

(m)

Figure – 53: Human body parts identification using skin color spaces (Considered only RGB model here) (a)Walking; (b) Standing; (c)Right hand rise;(d)Left hand rise; (e) Both hands rise; (f) Both hands up;(g)Right hand bend;(h) Left hand bend;(i)Right leg rise;(j) Left leg rise and; (k) Right salute; (l) Left salute(12); (m) Crouching

4.4.1 DISCUSSION ON HUMAN BODY PARTS IDENTIFICATION USING SKIN COLOR SPACE

The experimental results had been compared with two performance parameters. For the proposed six color space models, efficiency for a video and time consumption for one frame in various video sequences was evaluated. Also, the performance had been measured for the combination of color space models. Among the six models, the RGB based skin color model provided a higher performance than the other algorithms due to occurrence of more skin pixels whereas the YCbCr model gave less efficiency as in Figure 54 and Figure 55.

The time can be measured to compute the number of skin pixels for a frame in a video data. In the analysis, RGB color space model took additional time when compared to other color space algorithms. Due to more number of skin pixels, the RGB model took time such as 0.898, 0.901, 0.917, 0.918, 0.912, 0.903, 0.902, 0.903, 0.919, 0.925, 0.925, 0.921, 0.95, and 0.981 for thirteen activities. And the YCbCr

model required lesser time to evaluate the skin pixels. Table XVIII shows the time required to compute the skin pixels for the proposed six color space algorithms.

Moreover, the occurrence of pixels and efficiency were also calculated for the combined color space models. From the computation, the RGB has more efficiency whereas YCbCr has lesser performance. And the combined algorithm had been made with these combinations. In the first set, the combined RGB and YCbCr algorithm produces high efficiency whereas RGB and HSV2 gave lesser performance. And in the second set, RGB with the YCbCr model produced high performance and YCbCr with HSV2 gave less efficiency. The results of the combined algorithms had been shown in Figure 56-59.

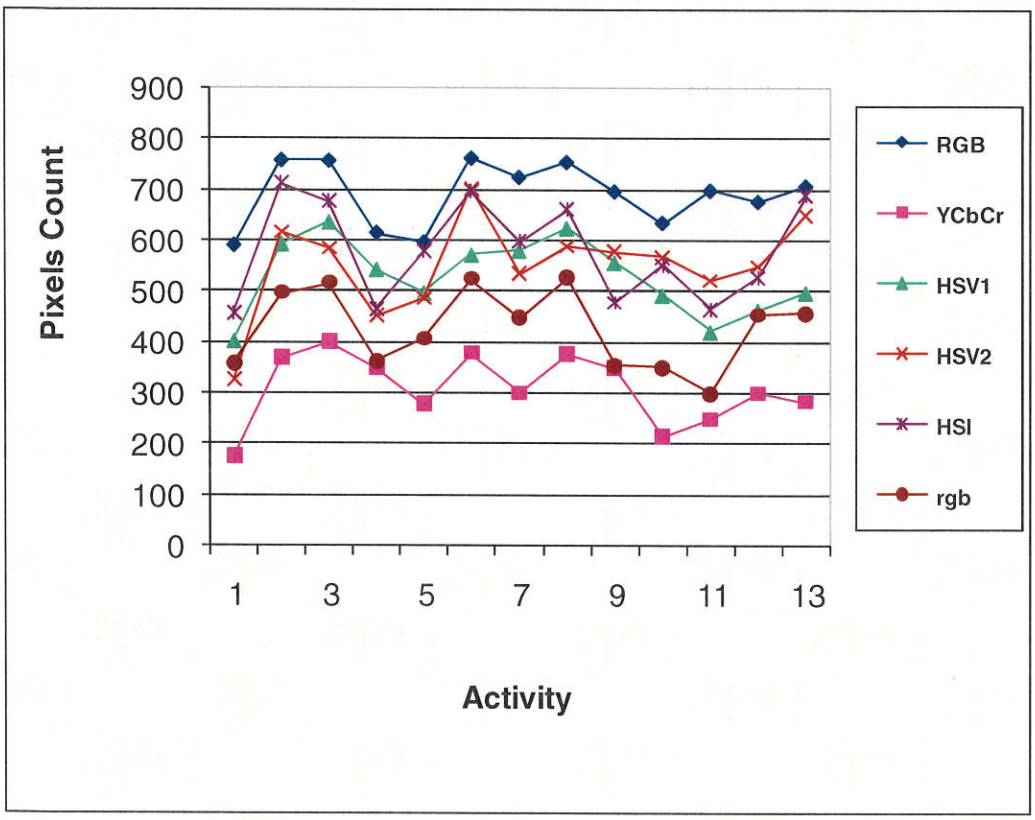

Figure – 54: Comparison of Pixels count in proposed RGB,YCbCr, HSV1, HSV2, HSI, and rgb color space algorithms. (Individual color spaces)

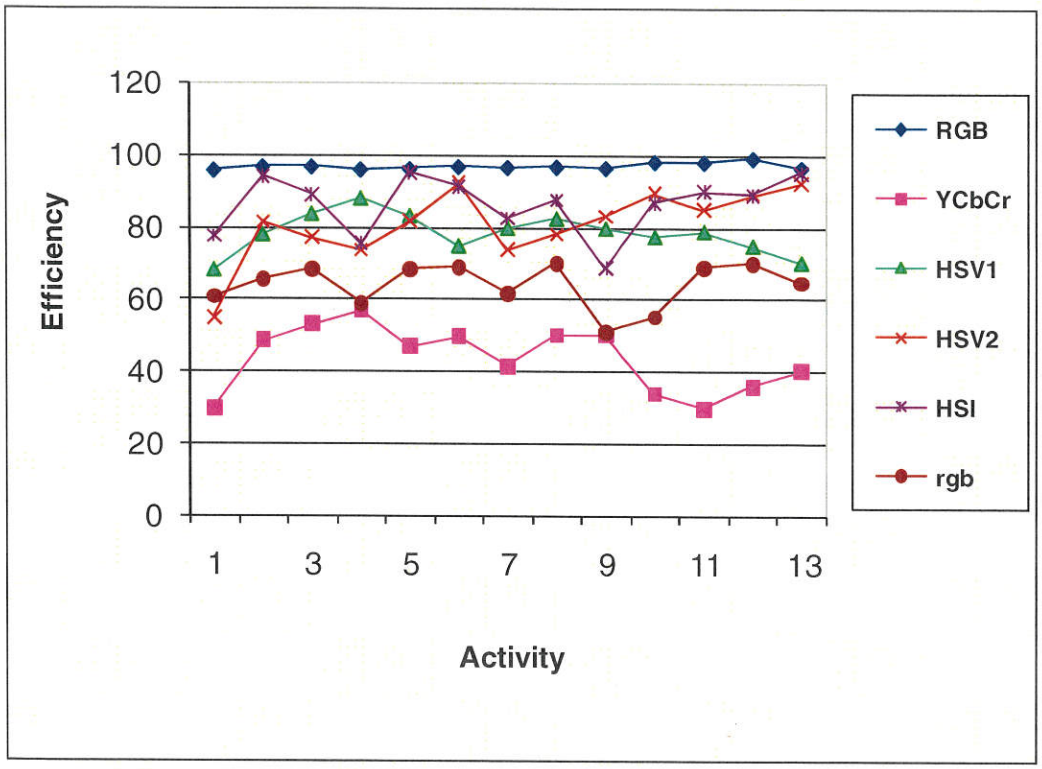

Figure – 55: Efficiency of proposed RGB, YCbCr, HSV1, HSV2, HSI, and rgb color space algorithms. (Individual color spaces)

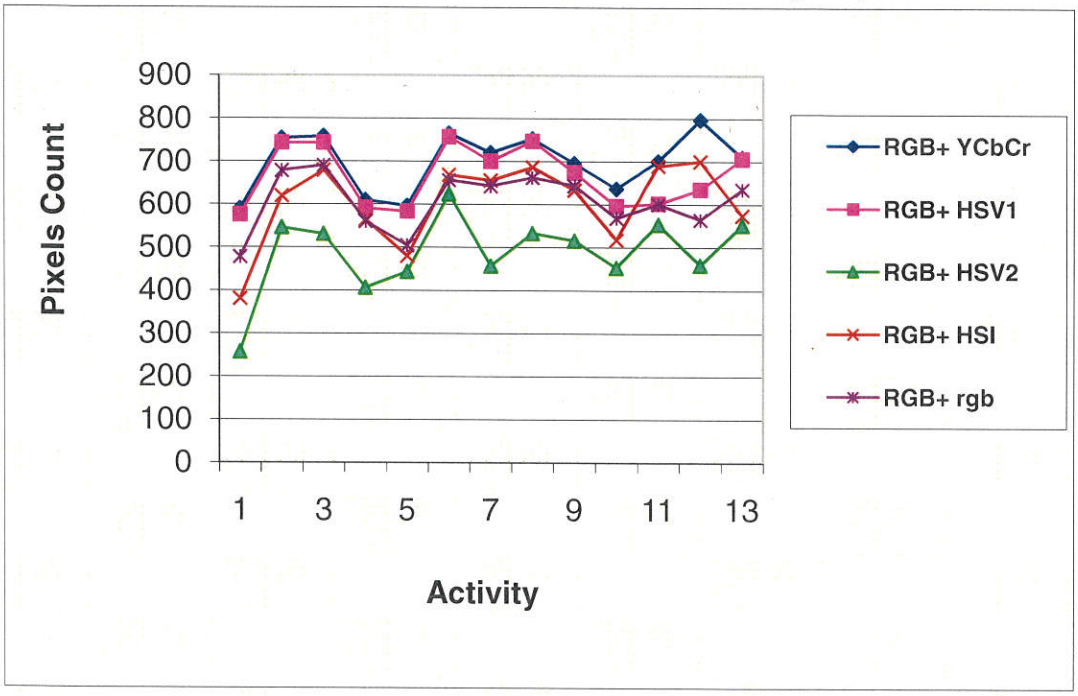

Figure – 56: Evaluation of pixels count in the proposed combined color space algorithms [RGB with YCbCr, HSV1, HSV2, HSI and RGB]

TABLE - XVIII

TIME REQUIRED TO COMPUTE SKIN PIXELS FOR A SINGLE VIDEO USING INDIVIDUAL COLOR SPACES (IN SEC)

Human poses	RGB	YCbCr	HSV1	HSV2	HSI	rgb (Normalized RGB)
1	0.898	0.826	0.856	0.864	0.877	0.861
2	0.901	0.838	0.873	0.872	0.895	0.882
3	0.917	0.831	0.856	0.871	0.897	0.87
4	0.918	0.845	0.865	0.873	0.881	0.72
5	0.912	0.813	0.852	0.861	0.885	0.87
6	0.903	0.825	0.873	0.883	0.895	0.73
7	0.902	0.835	0.875	0.81	0.911	0.85
8	0.903	0.827	0.87	0.875	0.87	0.867
9	0.919	0.817	0.81	0.87	0.886	0.821
10	0.925	0.823	0.851	0.85	0.889	0.78
11	0.921	0.82	0.75	0.85	0.895	0.866
12	0.95	0.81	0.88	0.8	0.869	0.85
13	0.981	0.82	0.81	0.875	0.876	0.831
Avg	0.919	0.825	0.847	0.858	0.886	0.830

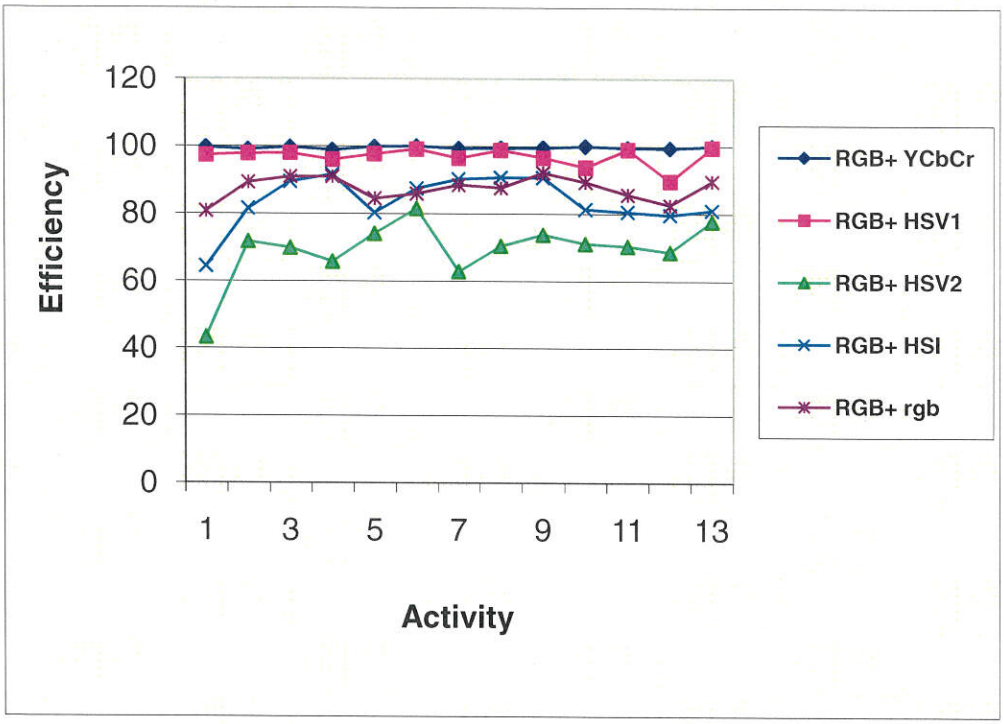

Figure – 57: Efficiency of proposed combined color space algorithms. [RGB with YCbCr, HSV1, HSV2, HSI and rgb]

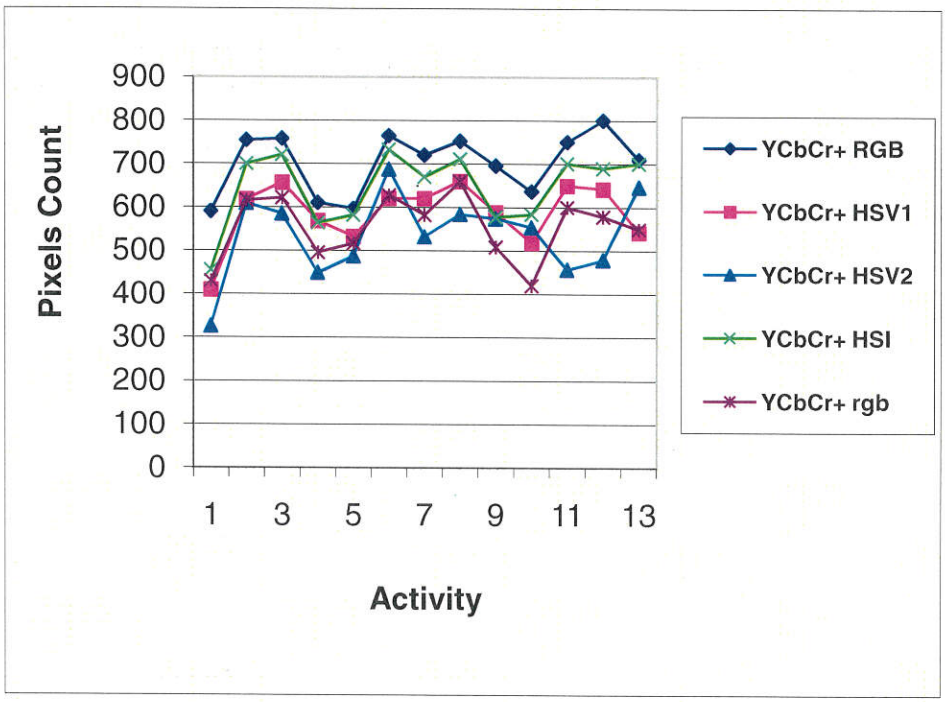

Figure – 58: Relationship of pixels count in the proposed combined color space algorithms [YCbCr with RGB, HSV1, HSV2, HSI and rgb]

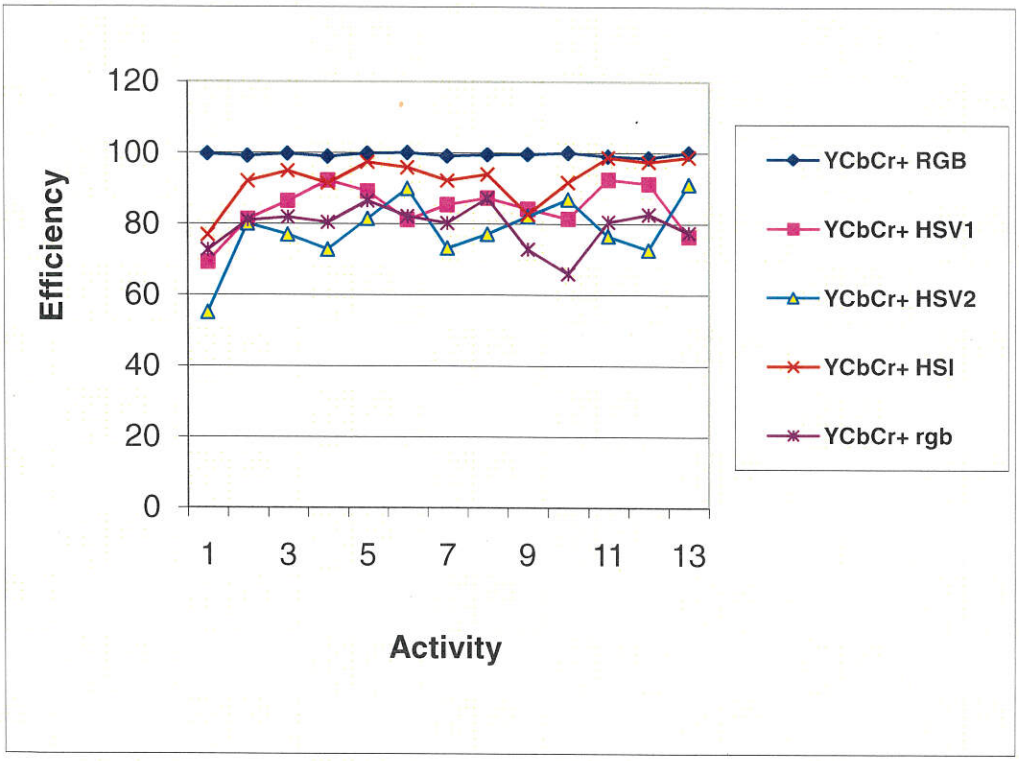

Figure – 59: Efficiency of proposed combined color space algorithms. [YCbCr with RGB, HSV1, HSV2, HSI and rgb]

4.5 RESULTS OF THINNING ALGORITHM

Figure 60 shows the results of the thinning algorithm for different poses.

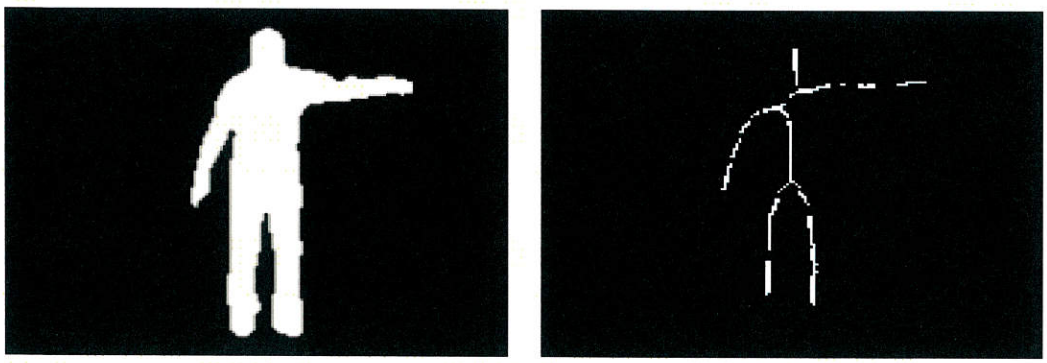

(a)

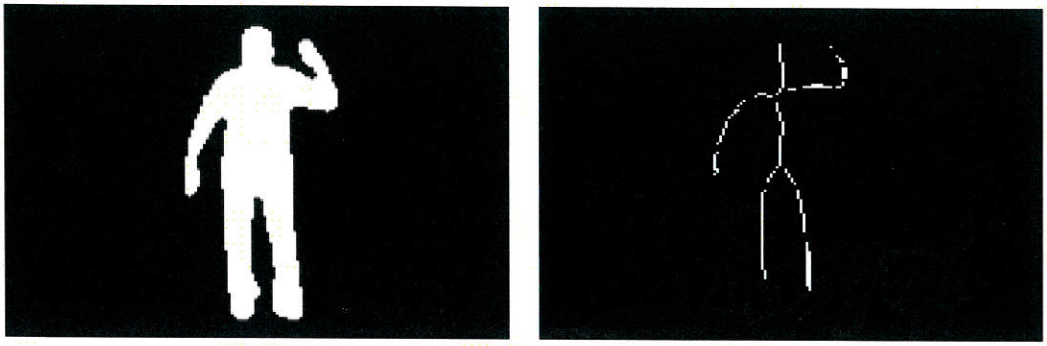

(b)

Figure – 60: Results of Thinning Algorithm

The next step was to develop the pose models for the human postures. After the human body parts were detected, the human pose models were constructed using the feature points in two dimensional (2D) views. The feature point was a point on the human body which was used to represent the body segments. The feature points that were derived from the human pose models play an important role in analyzing the activities.

4.5.1 RESULTS AND DISCUSSION ON HUMAN POSE MODELING

The proposed work had been developed using MATLAB 7.6(2008a) on Intel dual core processor, 2GB RAM and Windows XP SP2. The video sequences were acquired at the rate of 30 frames/second with the frame size of 320×240 pixels resolution. Figure 61 shows the simulation results of proposed work in which Column I indicates the original input video frame whereas Column II shows the two dimensional model of sports person.

1. Frame No: 1100

Column I

Column II

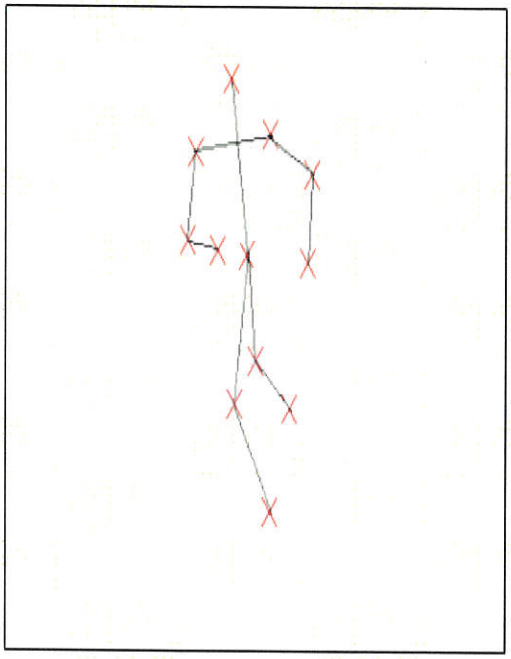

(a) Original video frame

(b) Human body model

2. Frame No: 1240

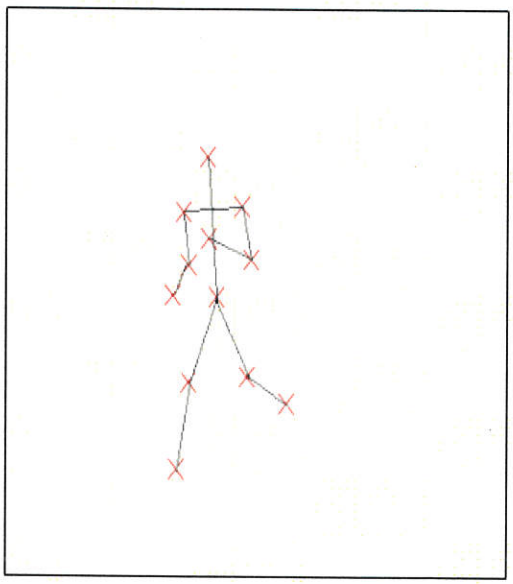

3. Frame No: 1546

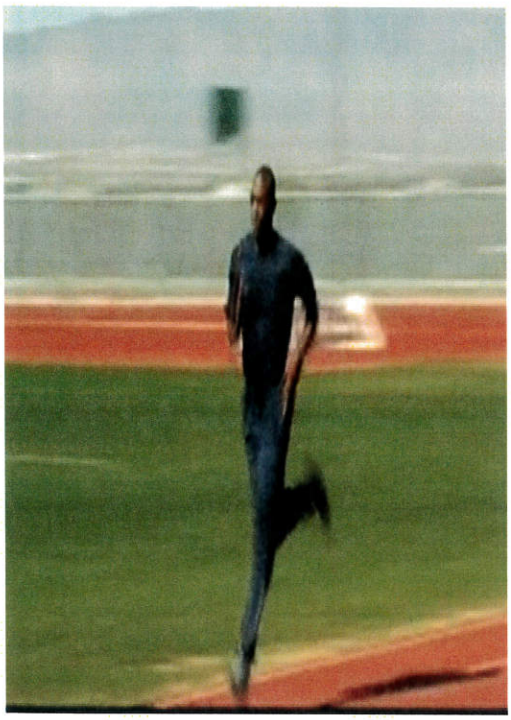

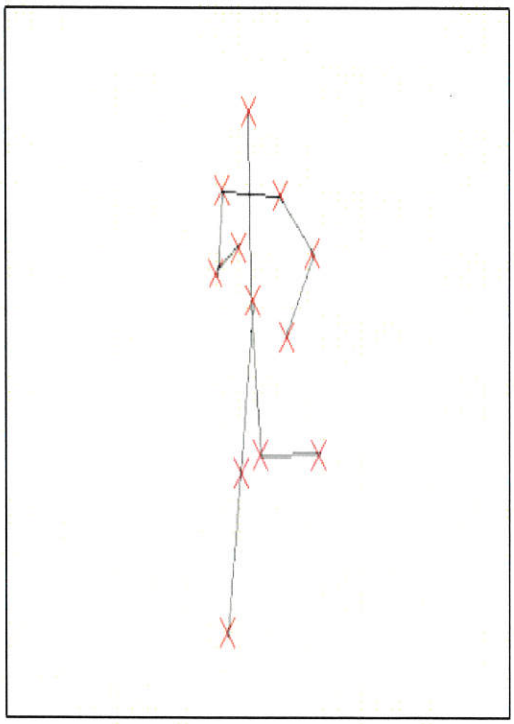

4. Frame No: 1678

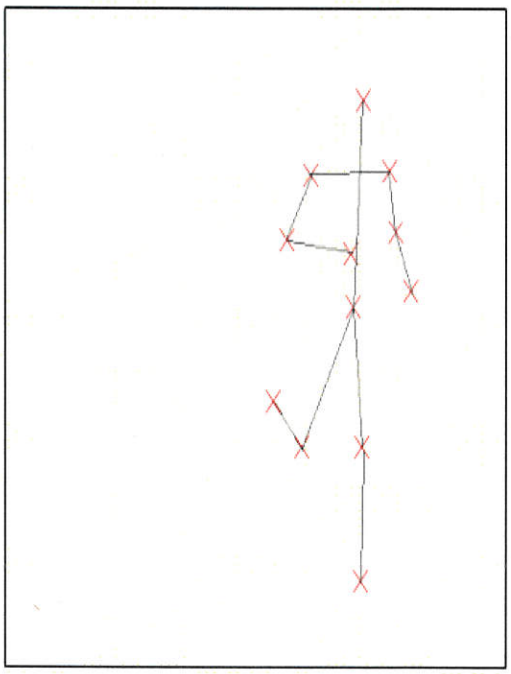

5. Frame No: 1700

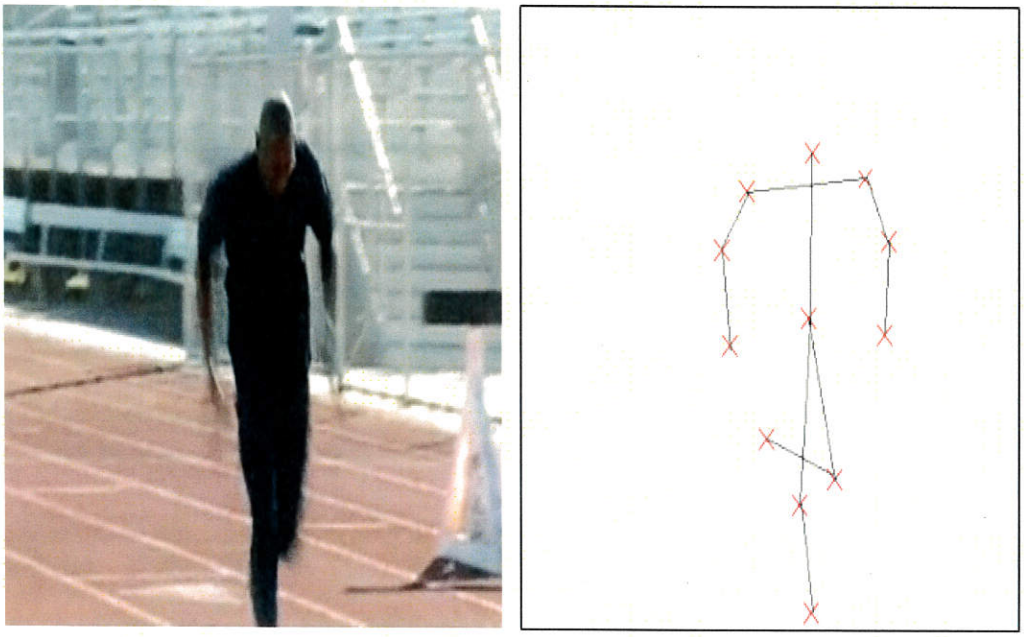

Figure – 61: Results of human body modeling

TABLE – XIX

EFFICIENCY OF 2D MODEL AND 3D MODEL FOR DIFFERENT VIDEOS

Videos	No. Of frames	No. of poses correct in 2D Modelling			3D Modelling	
		Stick Fig.	Cylinder	Efficiency (%)	No. of poses correct	Efficiency (%)
Video 1	1006	880	880	87.5	860	85.5
Video 2	1147	1026	1026	89.5	940	81.9
Video 3	1382	1275	1275	92.3	1200	86.8
Video 4	864	810	810	94.0	740	85.6
Video 5	1502	1400	1400	93.2	1250	83.2
Video 6	1257	1050	1050	83.5	1000	79.6
Video 7	1286	1100	1100	85.5	1100	85.5
Video8	671	650	650	96.8	600	89.4
Video 9	1600	1350	1350	84.4	1380	86.2
Video 10	1826	1590	1590	87.1	1570	85.9
Average				89.4	Average	85.0

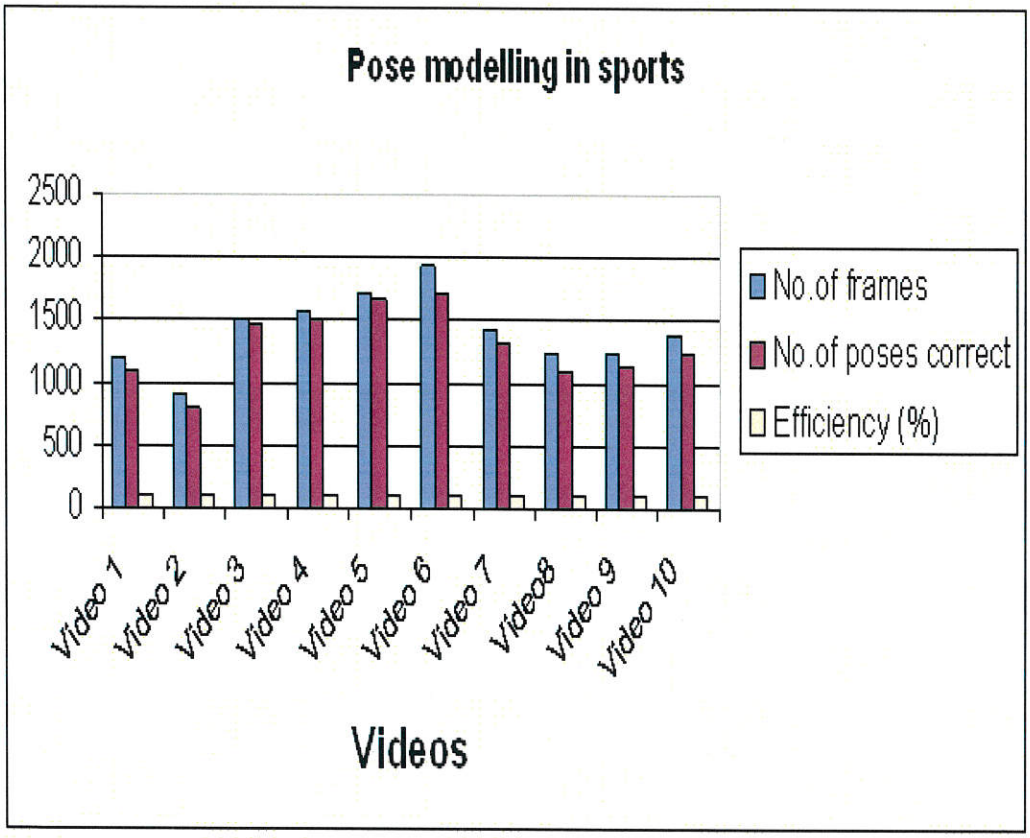

Figure – 62: Human pose analysis of different videos

Table XIX and Figure 62 shows the human pose analysis of various videos. Ten videos were considered for the analysis. The efficiency can be calculated using number of poses correctly detected with the help of an algorithm.

4.6 RESULTS AND DISCUSSION ON ANALYTICS IN SPORTS VIDEO

In this section, the developed human pose model was implemented on a running video after post model training and the various parameters like vertical Bounce, Stride angle, Stride length, Overstride angle, Toe lifting and Upperbody torque were analyzed.

Figure – 63: Athlete Running Video

Figure 63 shows the bouncing effect of runner head bobbing up and down. The over stride of the athlete tells that he is striking the ground first with his heel. This creates a fulcrum which puts a break on the critical velocity of the athlete and causes him to walk up. This slight distorted displacement and movement causes an hindrance to efficiency of movement. Newton's law of motion f = m x a is disturbed due to the distorted displacement as a result the flow of body movement is also disturbed.

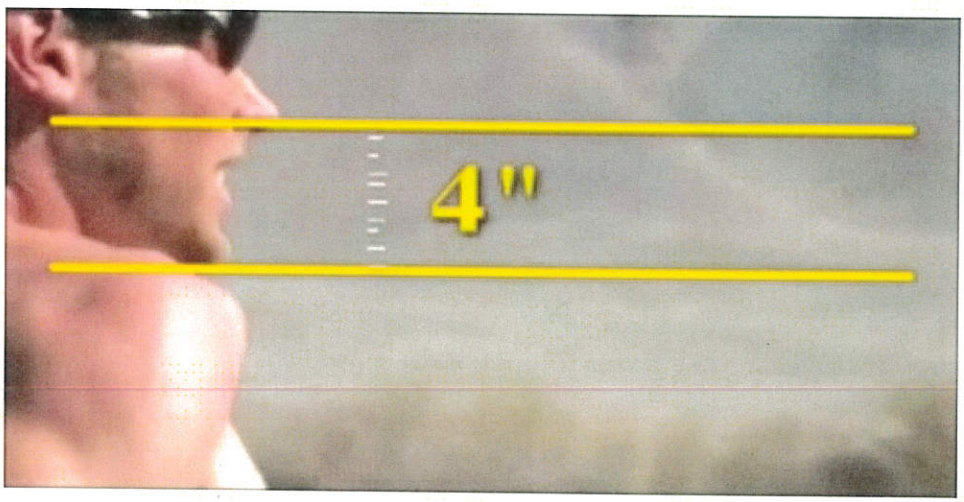

Figure – 64: Vertical Distance (Bounce)

Consider a Marathon of 26.2 miles horizontal distance (26,000 strides). Bounce means how much the runner moves up and down with each stride. Bounces indicated by a Line of 4" for each stride as shown in Figure 64.

For a total of 26,200 strides up times 4" is equal to 8725 vertical feet over 1.65 vertical miles. Similarly for 26,200 strides down times 4" will add another 1.65 miles to his marathon for a total of 3.3 additional grueling miles just from bouncing up and down.

Figure – 65: Bouncing up and down

Each time the athlete levels the vertical distance by up and down the athlete experiences twice the body weight as shown in Figure 65. So twice the body weight multiplied with the distance of 26,200 strides will equal to 6,812,000 pounds. This is the main source of fatigue in the marathon.

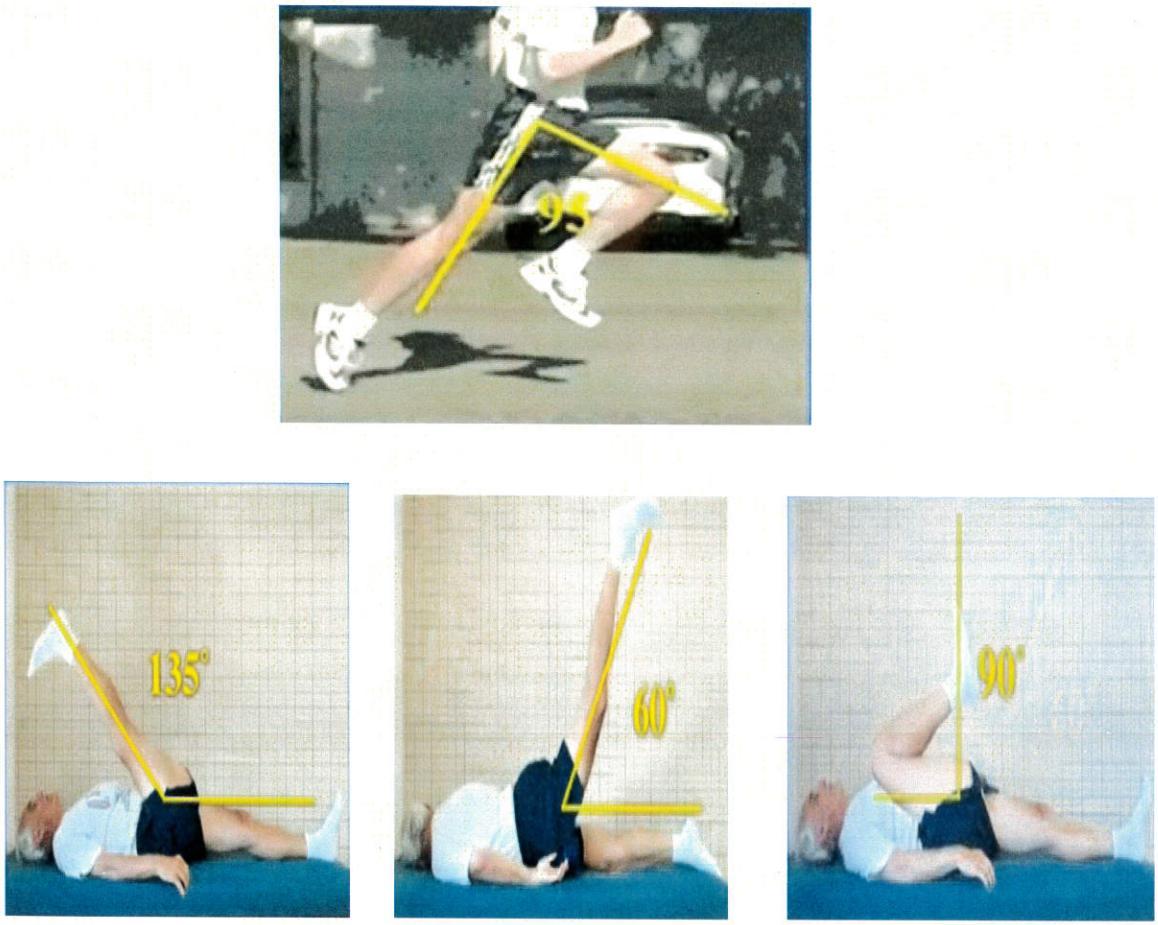

Figure – 66: Stride angle

Stride angle was mainly a function of leg and hip flexibility. A 30° increase in the stride angle enables the athlete to cover 60% more ground with each stride, simultaneously reducing the athletes bounce to half as shown in figure 66. For maximum stride angle and minimum balance for running, an athlete needs a 135° of hip leg range and 60° hip extension and 90° of hip flexibility.

The stride angle was the maximum opening between the front and trailing leg. Usually it is found that for every degree increase in stride angle the stride length increases by 2%.

(a) (b)

Figure – 67: Stride angle video (a) Stride angle of 90° (b) Stride angle of 106°

In Figure 67(a) the runner has a stride angle of 90° on his left side and 91° on his right side. Another person as shown in Figure 67(b) having stride angle of 106° covers 31% more ground with each stride he takes. Since he was having fewer strides he was also bouncing up and down. The overstride angle of the overleg is measured when the foot first touches the ground. For maximum efficiency a larger negative stride angle as shown in Figure 68 is needed. Increasing the stride was the fastest way to reduce overstride angle.

Figure – 68: Overstride angle

Many distance runner lift their toes as they run due to fine attention. Toe lift was the main source of shins function in runners as shown in Figure 69.

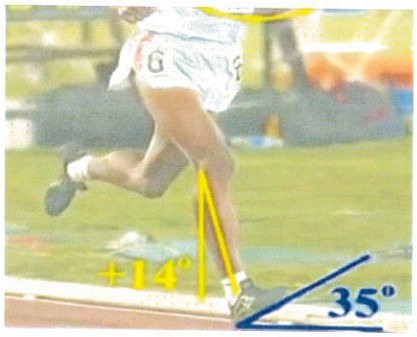

Figure – 69: Toe Lifting

Runner has a toe lift angle of 35°. Runners lifts their toes by contracting shin muscles, while the muscles of toe contracted, the heel touchdown. The forward motion shrinks the foot flat on the ground and this widely stretches the shin muscle while they are still contracted forcing the muscles to stretch over its contracted tears the muscle and in some cases it causes stretch fractures. It is discovered that most running injuries are caused by upper torque when the shoulders are tight, the upper body was twisted over torque to the right when the right hand goes back, this forces the left arm to swing across the body as shown in Figure 70. To compensate for this upper body torque, a runner has to swing the right leg over torque to a middle line.

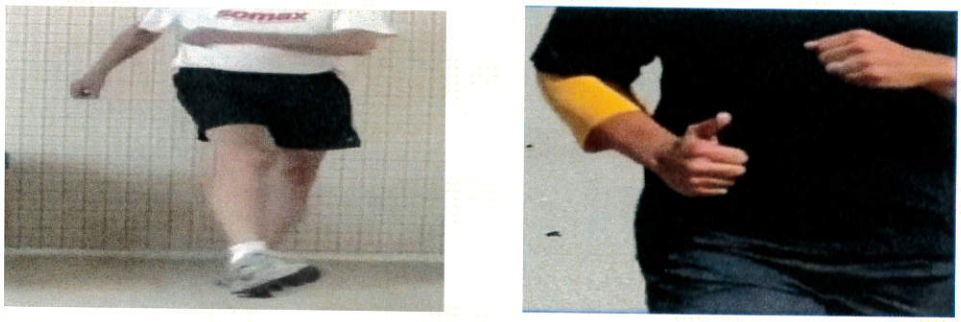

Figure – 70: Upper body torque